Shape Complexity in Turbulence

Haris J. Catrakis and Paul E. Dimotakis
Graduate Aeronautical Laboratories, California Institute of Technology, Pasadena, California 91125
(Received 4 September 1997)

The shape complexity of irregular surfaces is quantified by a dimensionless area-volume measure. A joint distribution of shape complexity and size is found for level-set islands and lakes in two-dimensional slices of the scalar field of liquid-phase turbulent jets, with complexity values increasing with size. A well-defined power law, over 3 decades in size (6 decades in area), is found for the shape complexity distribution. Such properties are important in various phenomena that rely on large area-volume ratios of surfaces or interfaces, such as turbulent mixing and combustion. [S0031-9007(97)05126-0]

PACS numbers: 47.27.–i, 02.50.–r, 47.53.+n

Structures observed in many phenomena exhibit a wide range of sizes and a variety of shapes [1–5]. In turbulence, in particular, the geometry of structures derived from level sets of scalar or vorticity fields in various flows has been a candidate for several descriptions [6–10]. In this Letter, a dimensionless measure of shape complexity based on surface (area) and volume properties is employed to analyze area-volume (perimeter-area, in 2D) properties of level sets of scalar fields in turbulent jets. Such statistics facilitate the description and modeling of turbulent mixing. In the context of chemical reactions and combustion in non-premixed hydrocarbon turbulent flames, for example, in which combustion is confined largely to the instantaneous stoichiometric (isoscalar) surface [11], area-volume measures of the isoscalar surface are required to relate the local burning rate to the time required for local consumption of unburnt fuel pockets. Such area-volume properties are also useful in the description of other phenomena that rely on large area-volume ratios of surfaces or interfaces, e.g., nephron cells possess complex boundaries to accommodate high flow rates in response to small osmotic gradients [12].

The geometric complexity of the shape of surfaces can be quantified by a dimensionless area-volume measure. For closed surfaces embedded in d-dimensional space ($d \geq 2$), size can be measured by $V_d^{1/d}$, where V_d is the volume enclosed by the surface. For a given size, the sphere has the least surface area,

$$S_{d,\mathrm{sph}} = \frac{1}{k_d} V_{d,\mathrm{sph}}^{(d-1)/d}, \quad \text{with } k_d = \frac{\Gamma^{1/d}(1 + d/2)}{d\pi^{1/2}}, \tag{1}$$

in terms of the sphere volume, $V_{d,\mathrm{sph}}$, where $\Gamma(x)$ is the gamma function. For any closed surface, the surface area S_d is then bounded from below, i.e.,

$$S_d \geq \frac{1}{k_d} V_d^{(d-1)/d}. \tag{2}$$

To examine area-volume behavior over a range of sizes, it is useful to normalize the surface area by the area of a sphere of equal size. The resulting area-volume measure, denoted here by Ω_d is a (dimensionless) measure of the complexity of the shape of the surface: Ω_d quantifies the departure of the shape (complexity) from its minimum value, i.e., it will be unity for spheres and unbounded from above,

$$1 \leq \Omega_d \equiv \frac{k_d S_d}{V_d^{(d-1)/d}} \leq \infty. \tag{3}$$

Nonrectifiable (e.g., fractal) surfaces would correspond, for example, to $\Omega_d = \infty$. For 2D closed contours, the size measure becomes the square root of the enclosed area, i.e., $V_2^{1/2} = A^{1/2}$, so that the 2D shape complexity becomes [cf. Eq. (1)]

$$1 \leq \Omega_2 \equiv \frac{k_2 P}{A^{1/2}} \leq \infty, \quad \text{with } k_2 = \frac{1}{2\pi^{1/2}}, \tag{4}$$

where $P = S_2$ is the perimeter of the contour. Ω_2 measures the bounding arc length per unit square root of the enclosed area.

Jet-fluid concentration fields measured in liquid-phase turbulent jets were analyzed at Reynolds numbers $\mathrm{Re} \simeq 4.5 \times 10^3$, 9.0×10^3, and 18×10^3 [9]. The jet plenum was seeded with disodium fluorescein which is a passive scalar with Schmidt number $Sc \equiv \nu/\mathcal{D} \simeq 1.9 \times 10^3$; ν is the kinematic viscosity of the fluid (water) and $\mathcal{D}$ is the scalar diffusivity. 2D spatial data of the scalar field were recorded in a plane normal to the jet axis, 275 nozzle diameters downstream of the jet exit, with laser-induced fluorescence and digital-imaging techniques. An example of such data at $\mathrm{Re} \simeq 9.0 \times 10^3$ is shown in Fig. 1 (top).

An example of a scalar level set, i.e., $c(x, y) = \text{const}$, at $\mathrm{Re} \simeq 9.0 \times 10^3$ is shown in Fig. 1 (bottom). The scalar threshold chosen corresponds to the peak (mode) of the jet-fluid-concentration probability density function (pdf), at this Re [9], with results found to be relatively insensitive to this choice. The level set consists of disjoint (closed) contours of different sizes and shapes. These contours are either "islands" or "lakes," depending on whether interior scalar values are higher or lower, respectively,—a "continent" can also be identified in

 0031-9007/98/80(5)/968(4)$15.00

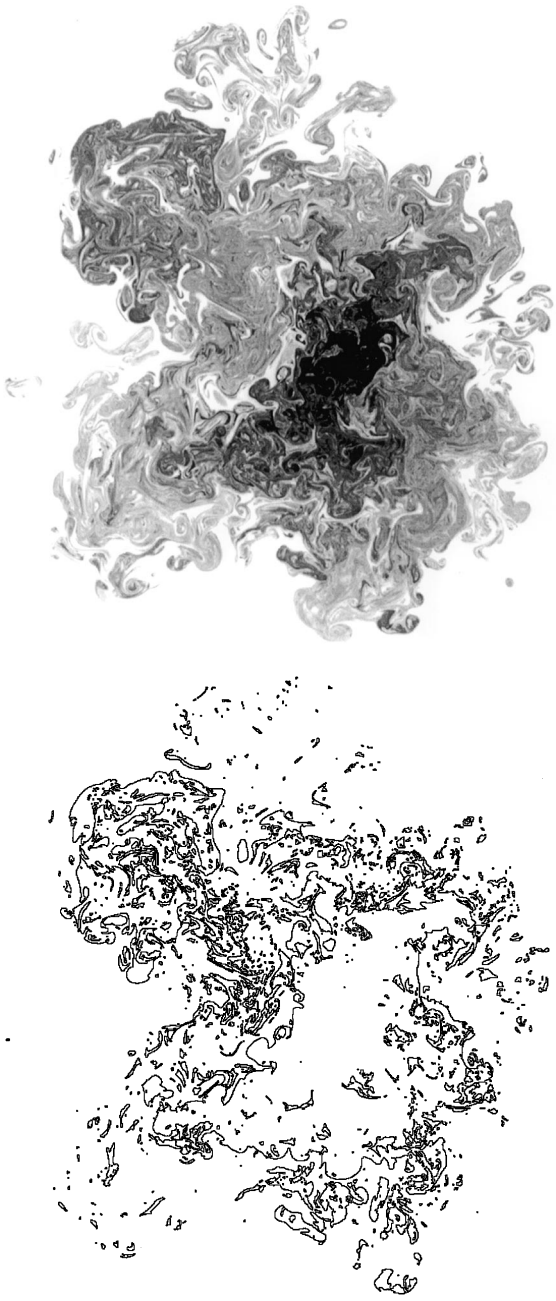

FIG. 1. Top: jet-fluid concentration in far field ($z/d_0 = 275$) of a liquid-phase turbulent jet at Re $\simeq 9.0 \times 10^3$. Increasing grey levels label increasing jet-fluid concentration values. Bottom: jet-fluid concentration level set thresholded at the mode of the scalar-field pdf. More than 700 islands and lakes, on average, are found in each such realization.

general. To compute the perimeter P and area A of the islands/lakes, level sets were extracted from the data with a local, biquadratic B-spline representation of the 2D $c(x, y)$ surface and a contour-tracking algorithm. This ensures C^1 continuity (no cusps) and eliminates pixelation artifacts of digital-image contour-extraction methods, such as maximum/minimum bounds for the pixelated perimeter [13]. The present method provides an estimate of the perimeter (and area) of the islands/lakes that will approach the level-set arc length in the limit of high resolution.

Following Lovejoy's area/perimeter analysis of cloud/rain regions [4], a scatter plot of normalized perimeter and size, P/δ_b and $A^{1/2}/\delta_b$, for turbulent-jet islands/lakes is shown in Fig. 2, for six image realizations at Re $\simeq 9.0 \times 10^3$ (cf. Fig. 1). Size/perimeter values for more than 4200 islands/lakes (over 700 islands/lakes per realization on average) are depicted, normalized by the (ensemble-averaged) outer scale of the level set δ_b computed as the square root of the bounding-box area [9]. The minimum perimeter for circles [cf. Eq. (2)] is indicated in Fig. 2 as a solid line. A power-law fit, $P/\delta_b \propto (A^{1/2}/\delta_b)^{q_2}$, is also shown (dashed line) using Lovejoy's value ($q_2 = 1.35$).

A scatter plot of the shape complexity Ω_2 and normalized size $A^{1/2}/\delta_b$ is shown in Fig. 3. The horizontal axis, i.e., $\Omega_2 = 1$, represents the minimum value of shape complexity (circles). The data indicate that Ω_2 approaches the minimum value (unity) at small sizes; near-circular shapes are encountered at the smallest (diffusion-dominated) scales.

Progressively larger values of Ω_2 are encountered with increasing size (Fig. 3). This finding can be appreciated, kinematically, by noting that the shape of a flow structure is subject to greater distortions, at its own scale, by smaller structures and, to a lesser extent, by larger structures. Accordingly, larger-sized structures may be expected to be more complex in shape, as they subtend a larger fraction of the range of spatial scales, in turbulent flows in general.

The data indicate that islands/lakes derived from 2D scalar level sets need to be characterized by a *joint distribution* of size and shape complexity, $\mathcal{W}_2(A^{1/2}/\delta_b, \Omega_2)$, i.e.,

$$\int_1^\infty \int_0^1 \mathcal{W}_2(A^{1/2}/\delta_b, \Omega_2) d(A^{1/2}/\delta_b) d\Omega_2 = 1 . \quad (5)$$

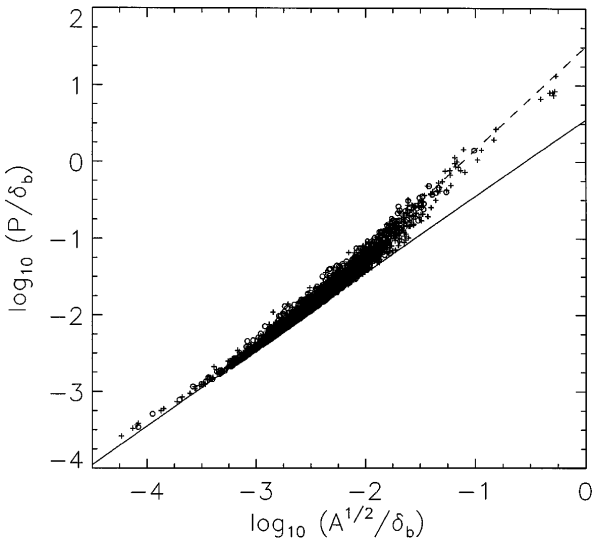

FIG. 2. Scatter plot of normalized perimeter, P/δ_b, vs normalized size, $A^{1/2}/\delta_b$, of isoscalar islands and lakes at Re $\simeq 9.0 \times 10^3$ (islands: crosses; lakes: circles).

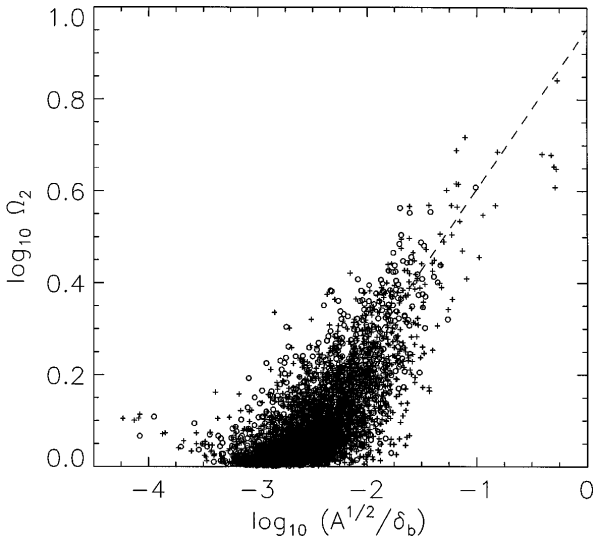

FIG. 3. Scatter plot of shape complexity, Ω_2, vs normalized size, $A^{1/2}/\delta_b$ (same data as in Fig. 2).

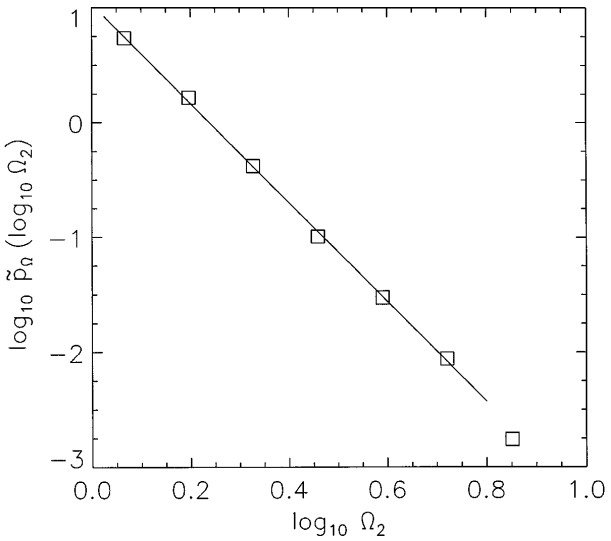

FIG. 4. Shape complexity pdf of islands and lakes. Solid line: power-law fit (in these coordinates).

The islands/lakes span, roughly, 3 decades in size, or 6 decades in area. Area-size behavior of contours derived from complex structures [4,5] has been modeled previously in terms of functional, power-law relations, e.g., $\Omega_2 \propto (A^{1/2}/\delta_b)^{q_2-1}$, where q_2 would be a constant; cf. dashed line in Fig. 3 for $q_2 = 1.35$ [4]. For stochastic processes in general, however, a joint distribution of shape complexity and size can be expected.

The present data show differences from power-law functional relations. Over most of the Ω_2 range, islands and lakes are found with sizes spanning more than 1 decade, or 2 decades in area, for a given shape complexity. Lovejoy's suggestion appears to capture the mean trend in Fig. 3 at large sizes. However, the most probable values of size and shape complexity lie on a curve (Fig. 3) for small sizes. Also, large lakes of high shape complexity are found, relative to the mean behavior, which can result in a substantially higher (total) shape complexity of the level set.

From such statistics, the size or shape-complexity pdf of the islands/lakes can be computed. The size pdf, corresponding to the projection of the joint pdf $\mathcal{W}_2$ on the size axis, i.e., $p_A(A^{1/2}/\delta_b) = \int_1^\infty \mathcal{W}_2(A^{1/2}/\delta_b, \Omega_2) d\Omega_2$, is nearly log normal at small scales [10]. It corresponds to a non-power-law Korčak distribution, $N_A(A^{1/2}/\delta_b) = \int_{A^{1/2}/\delta_b}^\infty p_A(x)dx$, where N_A is the count of islands/lakes of size greater than $A^{1/2}/\delta_b$ [1].

The pdf of shape complexity, $p_\Omega(\Omega_2)$, decreases with increasing Ω_2, as shown in Fig. 4. The Ω_2 values span almost 1 decade, i.e., there are islands/lakes with up to 10 times the perimeter, per unit (root) area, of equal-sized circles. The data indicate a power-law pdf of shape complexity, i.e.,

$$P_\Omega(\Omega_2) \propto \Omega_2^{-\nu}, \tag{6}$$

with $\nu \simeq 5.3$; the largest-Ω_2 (binned) value reflects the "continents" and was omitted in the fit. Near-circular contours correspond mostly to (diffusion-dominated) small-size features (cf. Fig. 3) and have the highest shape-complexity probability density. The power-law pdf of shape complexity is equivalent to an exponential pdf for $\ln \Omega_2$,

$$\hat{p}_\Omega(\ln \Omega_2) \propto e^{-(\nu-1)\ln \Omega_2}, \tag{7}$$

i.e., log-Poisson statistics [14,15], for exponents $\nu > 1$, with $\hat{p}_\Omega(\ln \Omega_2) \equiv \Omega_2 p_\Omega(\Omega_2)$. The constant ν is the mean logarithmic shape complexity, i.e., for these data, $\langle \ln \Omega_2 \rangle = 1/(\nu - 1) \simeq 0.23$, or $\langle \log_{10} \Omega_2 \rangle \simeq 0.10$.

Level-set data, such as in Fig. 1, show evidence of many lakes within the continent, several islands within those lakes, as well as lakes within those islands. This topology necessitates an extension of the (individual) shape-complexity measure [Eq. (4)]. The total perimeter $P_{\rm tot}$ and enclosed area $A_{\rm tot}$ of regions of the level set where the scalar field exceeds the threshold, i.e.,

$$\begin{aligned} P_{\rm tot} &\equiv \sum_{i=1}^{n_{\rm isl}} P_i^{\rm (isl)} + \sum_{i=1}^{n_{\rm lak}} P_i^{\rm (lak)}, \\ A_{\rm tot} &\equiv \sum_{i=1}^{n_{\rm isl}} A_i^{\rm (isl)} - \sum_{i=1}^{n_{\rm lak}} A_i^{\rm (lak)}, \end{aligned} \tag{8}$$

with the minus sign for lakes in the area definition, can be used to define the total shape complexity $\Omega_{2,\rm tot}$ as [Eq. (4)]

$$\Omega_{2,\rm tot} \equiv \frac{k_2 P_{\rm tot}}{A_{\rm tot}^{1/2}}, \tag{9}$$

which can also be expressed as a weighted sum of the (individual) shape complexities of the islands and lakes [cf. Eq. (8)].

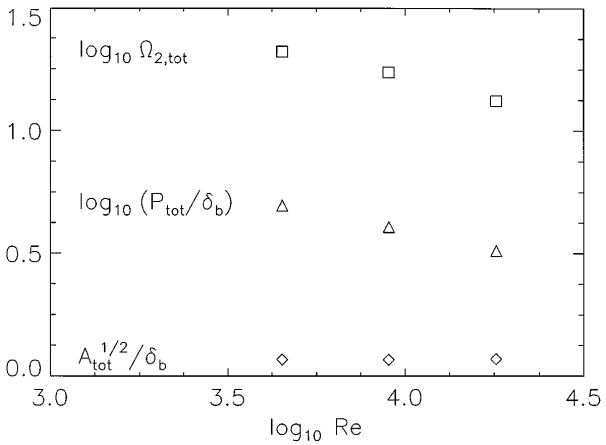

FIG. 5. Reynolds-number dependence of total area-perimeter measures, $\Omega_{2,\mathrm{tot}}$, $P_{\mathrm{tot}}/\delta_b$, and $A_{\mathrm{tot}}^{1/2}/\delta_b$.

The $\Omega_{2,\mathrm{tot}}$ measure is the ratio of the (total) isoscalar interfacial length to the (square root of the) total area of the scalar-field cross section, where jet fluid has not yet mixed down to the scalar-threshold value. In the context of non-premixed jet hydrocarbon combustion, for example, the $\Omega_{2,\mathrm{tot}}$ measure evaluated at a threshold chosen to coincide with the stoichiometric fuel-to-air mixture fraction would be the perimeter-to-root-area ratio of the burning, isoscalar interface.

The Reynolds-number dependence of the total area-volume measures for the present data, $\Omega_{2,\mathrm{tot}}$, $P_{\mathrm{tot}}/\delta_b$, and $A_{\mathrm{tot}}^{1/2}/\delta_b$, is shown in Fig. 5. The total shape complexity *decreases* with increasing Re, with values of $\Omega_{2,\mathrm{tot}} \simeq 21$, 17, and 13, at the three Re values investigated, respectively. This particular turbulent flow, in other words, is found to generate scalar level sets of 2D shape complexity as high as 20 times that of a circle [cf. Eqs. (8) and (9)]. The decreasing complexity with increasing Re reflects the decreasing level-set length (Fig. 5), while the normalized size appears to be only weakly dependent on Re. This is in accord with other scalar measures in this Re range [9], and indicates increased (molecular-diffusion) mixing with increasing Reynolds number, relative to stirring, at least in liquid-phase-jet turbulent flows.

In conclusion, shape complexity is a dimensionless area-volume ratio which is useful in the analysis of geometric properties of complex surfaces, or interfaces, generated by turbulent flows and their relation to mixing and stirring. The present data on liquid-phase turbulent jets exhibit a joint distribution of size and shape complexity, with complexity values that increase with size. A power-law pdf of shape complexity was found for this flow. The general behavior of these measures may also be expected in other turbulent flows, with an outer-scale (continent) behavior that may generally be different (no larger scales). These measures are useful in modeling surfaces or interfaces in turbulent flows, as well as in other complex phenomena, in general.

Support under AFOSR Grant No. F49260-94-1-0353 and discussions with C. Bond, M. Cross, H. Lam, and A. Leonard, as well as assistance by G. Gornowicz with the *B*-spline representation of the scalar fields, are gratefully acknowledged.

[1] J. Korčak, Bull. Inst. Inter. Stat. **III**, 295–299 (1938).
[2] H. Steinhaus, Coll. Math. **III**, 1–13 (1954).
[3] B. B. Mandelbrot, Science **155**, 636–638 (1967).
[4] S. Lovejoy, Science **216**, 185–187 (1982).
[5] B. B. Mandelbrot, *The Fractal Geometry of Nature* (Freeman, NY, 1982).
[6] K. R. Sreenivasan, Annu. Rev. Fluid Mech. **23**, 539–600 (1991).
[7] P. Constantin, I. Procaccia, and K. R. Sreenivasan, Phys. Rev. Lett. **67**, 1739–1742 (1991).
[8] I. Procaccia, A. Brandenburg, M. H. Jensen, and A. Vincent, Europhys. Lett. **19**, 183–187 (1992).
[9] H. J. Catrakis and P. E. Dimotakis, J. Fluid Mech. **317**, 369–406 (1996).
[10] H. J. Catrakis and P. E. Dimotakis, Phys. Rev. Lett. **77**, 3795–3798 (1996).
[11] S. P. Burke and T. E. W. Schumann, Ind. Eng. Chem. **20**(10), 998 (1928).
[12] D. Welling, J. Urani, L. Welling, and E. Wagner, Cell Physiol. **39**, 953–963 (1996).
[13] P. N. Brandt, R. Greimel, E. Guenther, and W. Mattig, in *Applying Fractals in Astronomy*, edited by A. Heck and J. M. Perdang (Springer, Berlin, 1991), pp. 77–96.
[14] B. Dubrulle, Phys. Rev. Lett. **73**, 959–962 (1994).
[15] Z. S. She and E. C. Waymire, Phys. Rev. Lett. **74**, 262–265 (1995).